The Dissipation of a Left-Moving Cell in a Severe Storm Environment

LEWIS D. GRASSO

Cooperative Institute for Research in the Atmosphere, Fort Collins, Colorado

(Manuscript received 29 April 1999, in final form 15 October 1999)

ABSTRACT

Observations have shown that thunderstorms sometimes undergo updraft splitting, where one updraft moves to the right of the mean tropospheric wind and the other to the left. Observations also show that the left-moving updraft tends to dissipate approximately 15 min after the splitting process. The right-moving cell, however, may exist for up to a few hours.

Idealized modeling studies suggest that this behavior is related to the clockwise turning of the environmental shear vectors with height. The interaction between the environmental shear and the storms updraft produces a high–low pressure couplet oriented downshear. This pressure pattern produces favorable vertical accelerations for the right mover. This same process inhibits upward motion for the left mover.

In this paper an idealized simulation is presented that suggests an additional process that contributed to the decay of the left-moving updraft. Analysis of low-level storm-relative winds for the left-moving cell indicated that the inflow was from the cool precipitating downdraft. This inflow was characterized by negatively buoyant air. Subsequently the updraft dissipated approximately 1500 s after the precipitating downdraft formed. In contrast, the inflow for the right-moving updraft was partly from the downdraft and the undisturbed environment. A second simulation was run in which no precipitation was allowed to form, thus no downdraft formed. In that simulation the left mover was long lived. These results suggest that the simulated left-moving cell dissipated by ingesting downdraft air.

1. Introduction

Numerical simulations have shown that updraft splitting is influenced by the midlevel pressure field. Schlesinger (1980) and Rotunno and Klemp (1982, 1985) successfully demonstrated that this pressure field enhances lifting on the flanks of the presplit updraft. In time left- and right-moving updrafts, relative to the mean tropospheric flow, form. Generally, after the splitting process is complete, the left-moving updraft dissipates.

There is observational evidence that right-moving storms are more common than left-moving storms (Davies-Jones 1985). Environments characterized by shear vectors veering with height have been proposed to explain this difference (Rotunno and Klemp 1982). In their study they show that in a linearized setting the perturbation pressure field is proportional to $\mathbf{S} \cdot \nabla_h w$, where $\mathbf{S}$ and w are the constant environmental vertical shear of the horizontal wind vector and time varying vertical motion. This relationship was used to show that a high–low pressure couplet forms along the downshear direction. When the shear vectors veer with height, high pressure is located above low pressure on the northern flank of the left-moving updraft. The resulting vertical profile of pressure acts to inhibit upward motion within the left-moving updraft.

A long-lived left-moving thunderstorm was observed 3 April 1964. In an idealized simulation of that event, Wilhelmson and Klemp (1981) concluded that the low-level veering of the shear vectors slowed the development of the left mover. They also showed that the convergence along the gust front was necessary for the longevity of that simulated storm. They suggested that the lifting along the gust front was large enough to compensate for the adverse effect of the pressure field. This process was demonstrated by rerunning their simulation without rainfall. In this case, the left mover decayed soon after splitting from the parent cell. Similarly, Weisman and Klemp (1984) showed that a simulated left-moving cell survived in an environment with shear vectors that turned clockwise with height. In that study they demonstrated the importance of lifting along the expanding outflow boundary beneath the left mover.

These past studies show that when the environmental shear vectors veer with height an adverse environment for left-moving updrafts is produced. Enhanced lifting along the northern flank of the left-moving updraft is lost due to the linear pressure response of the environmental shear and updraft. This generally leads to the dissipation of the left mover.

Corresponding author address: Dr. Lewis D. Grasso, NOAA/NESDIS/RAMMT CIRA, Colorado State University, West Laporte Avenue, Fort Collins, CO 80523.
E-mail: grasso@genesis.cira.colostate.edu

In this study, an idealized numerical model simulation was performed to reevaluate the storm-splitting process. The current simulation was designed and initialized in a manner similar to that of the previous numerical experiments mentioned above. A sounding that is typical of a severe storm environment of the U.S. High Plains was used to initialize the domain. The simulated environment was characterized by shear vectors that veered with height below approximately 2 km and backed above. Convection was triggered through the use of a warm bubble. Results show that the left-moving updraft decayed shortly after splitting. When precipitation was not allowed to fall, the left-moving updraft did not decay shortly after splitting. It existed for 7200 s. This result suggests that the linear effect associated with the interaction of the veering environmental shear vectors and the updraft was not the cause for the dissipation of the left mover. In the left mover storm-relative frame, the low-level inflow was from the cool precipitating downdraft. Results suggest that the decay of the left mover was a result of the low-level updraft ingesting cool downdraft air. This study is an extension of previous work, introducing another process that may cause some left-moving updrafts to decay shortly after updraft splitting. General conclusions about observed storms cannot be made based on this one simulation. More simulations are required to evaluate the feasibility of the mechanism proposed in this paper.

This paper is subdivided into six main sections. Section 2 discusses the computational methodology. Results from the simulation with precipitation are presented in section 3. A second simulation was run with no precipitation; results are found in section 4. A discussion of the results are contained in section 5. Section 6 contains the summary and conclusions.

2. Computational methodology

The numerical model used for this simulation was version 3b of the Regional Atmospheric Modeling System developed at Colorado State University (Pielke et al. 1992). The following features of the model were used.

- A nonhydrostatic and compressible formulation (Tripoli and Cotton 1982) was used.
- A hybrid timestep scheme was used. Momentum was advanced using a leapfrog scheme while scalars were advanced using a forward scheme. Both used second-order advection.
- Vertical and horizontal turbulence was parameterized using a Smagorinsky deformation based eddy viscosity (Smagorinsky 1963) with stability modifications (Lilly 1962).
- A bulk microphysical scheme was used that included the following hydrometeor species: cloud droplets, rain droplets, aggregates, grauple, hail, snow, and pristine ice (Walko et al. 1995). Mixing ratios were predicted for these species except for pristine ice where both concentration and mixing ratio were predicted and cloud droplets where the mixing ratio is diagnosed.
- Other prognostic variables were the three components of momentum, u, v and w, Exner function π, total water r_t and ice-liquid potential temperature θ_{il} (Tripoli and Cotton 1981).
- Arakawa fully staggered C grid (Arakawa and Lamb 1981).
- Exner function tendencies used to update the momentum variables were computed using a time split scheme, similar to Klemp and Wilhelmson (1978).
- Lateral boundaries used the Klemp–Wilhelmson condition in which the normal velocity component specified at the lateral boundary is effectively advected from the interior.
- A wall was specified at the top boundary with a friction layer below.

Horizontal grid spacing of 2 km was used within a domain expanding 200 km $\times$ 200 km. Vertically the domain extended to a height of 24 km. The vertical grid spacing started at 100 m and was stretched by a factor of 1.1 until the level where it was 2000 m. From that height to the top of the domain the vertical grid spacing was held at 2000 m. The sounding in Fig. 1 was used to initialize the horizontally homogeneous storm environment. This sounding was extracted from a numerical simulation of 26 April 1991 over central Oklahoma. The sounding is characterized by moderate amounts of instability and clockwise turning of the shear vectors with height from the surface to approximately 2 km. The magnitude of the average vertical shear in the lowest 5 km was 4.5×10^{-3} s^{-1}. This sounding differs with those of previous idealized studies. Previous studies have used hodographs that turn clockwise from the surface to approximately 3–4 km with unidirectional shear above. The hodograph used in this study curved clockwise from the surface to near 2 km and turned counterclockwise above. The simulation extended over a 2-h period with a time step of 5 s.

Convection was triggered by an instantaneous warm bubble. The interior of the bubble had a spacially constant temperature excess of 3 K and a spacially constant 20% increase in water vapor. The bubble was 9 $\times$ 9 points in the horizontal and extended upward from 50 to 2600 m. This approach is similar to that of Grasso and Cotton (1995). Two additional simulations were conducted in which the bubble size was reduced to 7 $\times$ 7 and 5 $\times$ 5 points in the horizontal, to test the sensitivity of the results to the initial conditions. All other aspects of these simulations were the same as the 9 $\times$ 9 case. The morphology of the left mover in the two additional runs were similar to the one presented in this paper.

3. Simulated convection with precipitation

The evolution of the simulated convection was similar to previous studies in that the initial cell developed from

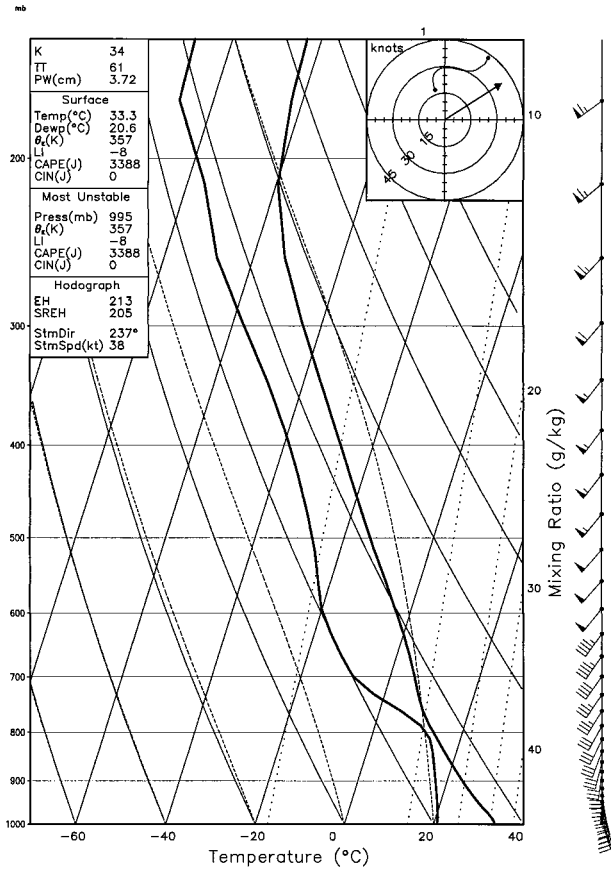

FIG. 1. Sounding used to initialize the simulation. Estimated motion of the right-moving cell is depicted by the arrow in hodograph.

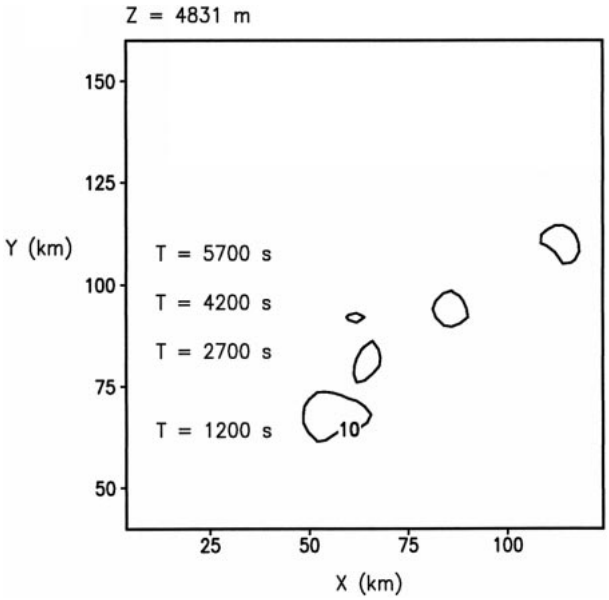

FIG. 2. Time sequence of the 10 m s^{-1} vertical velocity contour between 1200 and 5700 s at 4831 m.

the rising bubble. Splitting of the updraft began at approximately 1800 s. Once complete, the left- and right-moving updrafts began to diverge from one another. The left mover decayed by 3300 s, while the right-moving updraft continued to traverse the domain. A time sequence of the updraft at 4831 m is displayed in Fig. 2. The times corresponding to the four updraft locations are indicated on the left side of the domain. The northern updraft at 2700 s was the left mover.

Examination of the terms in the vertical equation of motion show that the two dominant forcings result from vertical gradients in π^*, $-\theta_0 \partial \pi^*/\partial z$, and numerical buoyancy, $B = [(\theta_v - \theta_0)/\theta_0 - r_c]g$. In the last two expressions θ_0, π^*, θ_v, r_c, and g represent the base state potential temperature, perturbation Exner function, virtual potential temperature, total water condensate mixing ratio, and the acceleration due to gravity, respectively. Figure 3 shows the sum of both forcing terms superimposed with vertical motion near 2 km between 1500 and 3000 s. At 1500 s, Fig. 3a, one region of maximum upward motion and lifting existed. Regions of updraft and upward forcing extended northward as the splitting process began. From 1800 to 2100 s (Figs. 3b,c) two updraft and upward lifting regions developed as splitting completed. Lifting associated with the left mover, however, decreased continuously from 2100 to 3000 s (Figs. 3d–f). By 3300 s, the left mover had dissipated.

Vertical forcing of vertical motion generated from $-\theta_0 \partial \pi^*/\partial z$ is displayed in Fig. 4. Between 1500 and 1800 s (Figs. 4a,b) there was no evidence that the updraft was forced by vertical gradients of π^*. Between 2100 and 3000 s (Figs. 4c–f) upward forcing did develop on the right side of the left-moving updraft. The magnitude of upward lifting, on the right side of the left mover, appeared to increase between 2100 and 2400 s, remaining somewhat constant between 2400 and 2700 s before decreasing by 3000 s. A region of downward forcing rotated clockwise around the left side of the left mover between 2100 and 2700 s. Between 2700 and 3000 s, the region of downward forcing moved northwest away from the left-moving updraft. A comparison of the upward lifting between the left- and right-moving updrafts showed that larger lifting was associated with the right mover (Figs. 4c–f). This difference might be accounted for by the clockwise turning of the hodograph below 2 km. Linear theory would predict larger upward lifting by vertical gradients of π^* associated with the right mover.

Positive buoyant forcing existed within the region of upward motion between 1500 and 1800 s (Figs. 5a,b). Comparing these two figures with Figs. 4a and 4b suggests that the updraft was still responding to the initial warm bubble during that time. As storm splitting completed, two regions of upward buoyant forcing existed within the left- and right-moving updrafts (Figs. 5c,d).

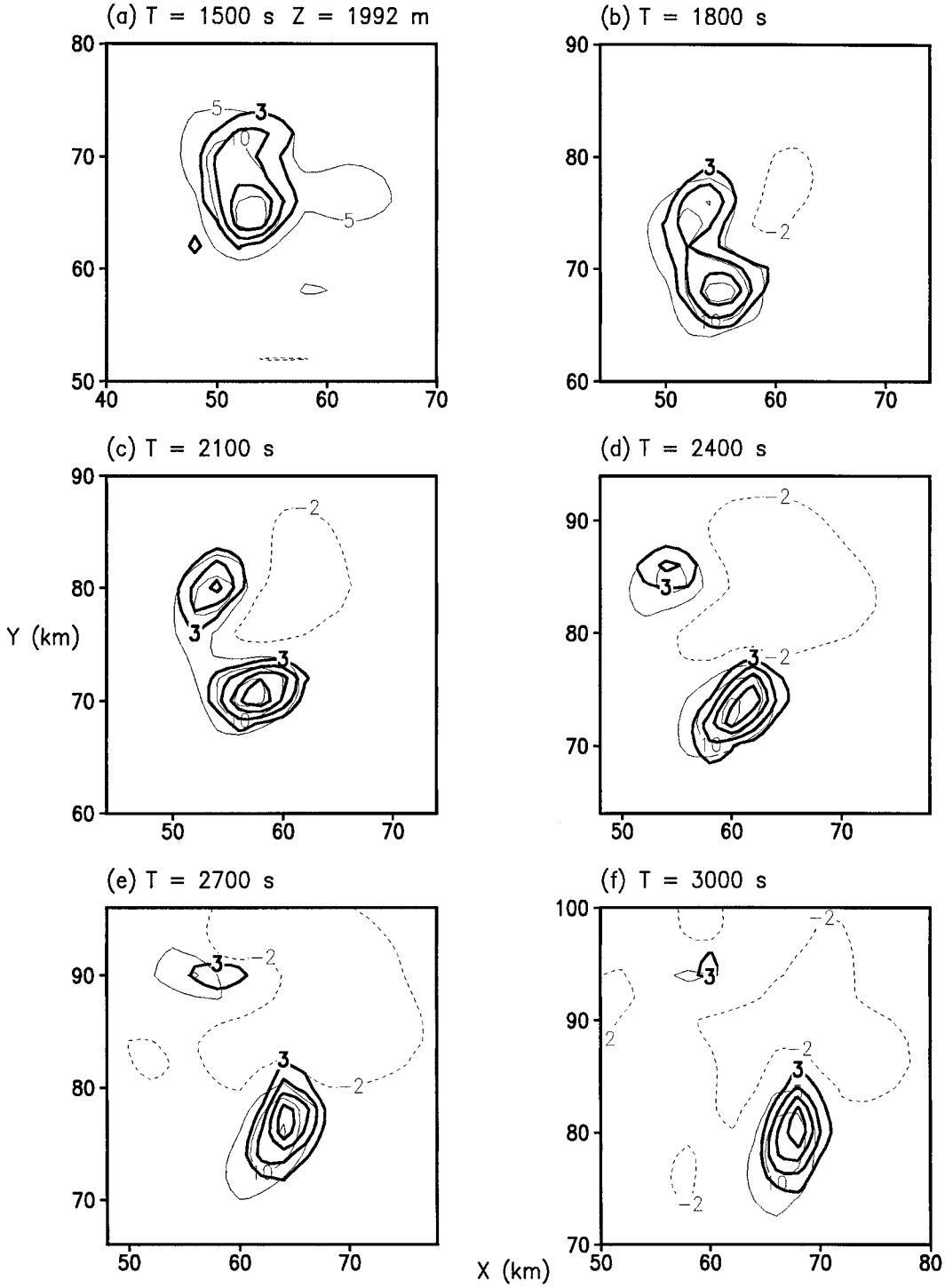

FIG. 3. Vertical motion (contoured every 5 m s^{-1}), thin contours, along with $\{-\theta_0 \partial \pi^*/\partial z + [(\theta_v - \theta_0)/\theta_0 - r_c]g\} \times 10^2$ (contoured every 3 m s^{-2}), thick contours, from (a) 1500, (b) 1800, (c) 2100, (d) 2400, (e) 2700, and (f) 3000 s at 1992 m.

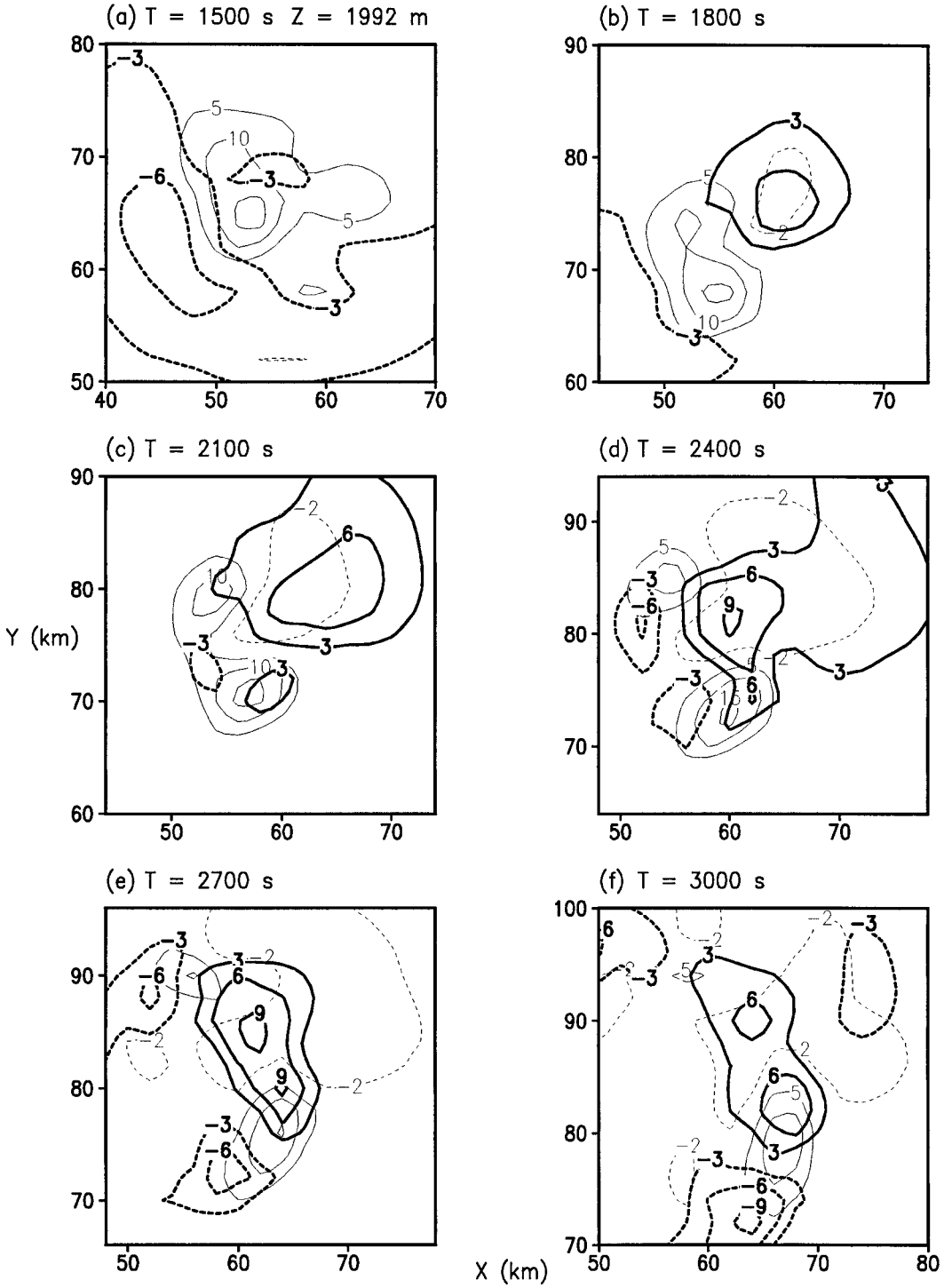

FIG. 4. Vertical motion (contoured every 5 m s^{-1}), thin contours, along with $(-\theta_0 \partial \pi^*/\partial z) \times 10^2$ (contoured every 3 m s^{-2}) thick contours, from (a) 1500, (b) 1800, (c) 2100, (d) 2400, (e) 2700, and (f) 3000 s at 1992 m.

While updraft splitting completed the values of upward buoyant forcing began to decrease within the left mover. From 2100 to 2700 s the magnitude of upward buoyant forcing reduced by approximately a factor of 2. Upward buoyant forcing within the right mover remained somewhat steady during the same time period. By 3000 s (Fig. 5f) the region of upward buoyant forcing moved northwestward and away from the left-moving cell.

Results displayed in the previous three figures suggest the total upward forcing between 1500 and 2100 s (Figs.

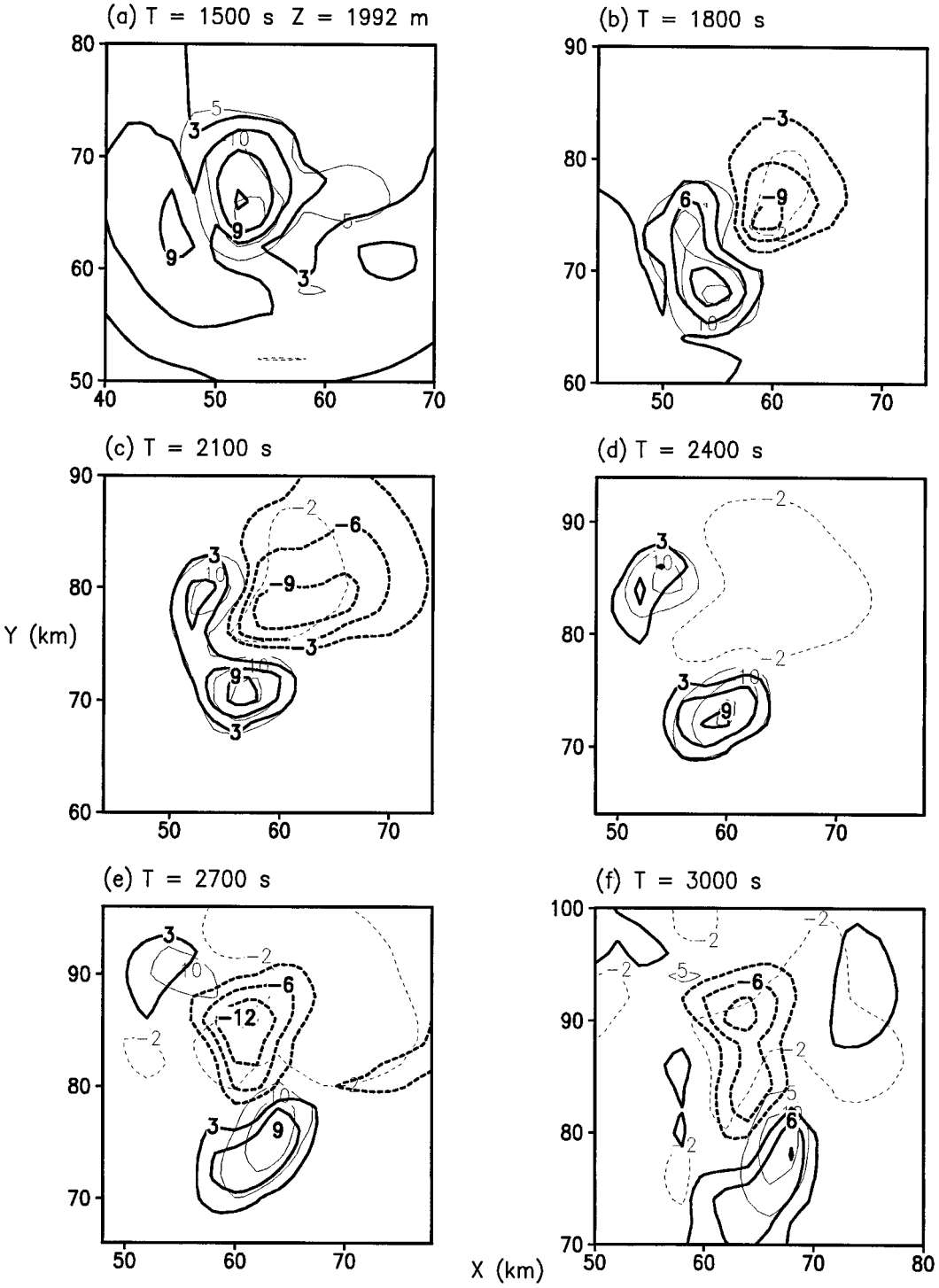

FIG. 5. Vertical motion (contoured every 5 m s^{-1}), thin contours, along with $\{[(\theta_v - \theta_0)/\theta_0 - r_c]g\} \times 10^2$ (contoured every 3 m s^{-2}), thick contours, from (a) 1500, (b) 1800, (c) 2100, (d) 2400, (e) 2700, and (f) 3000 s at 1992 m.

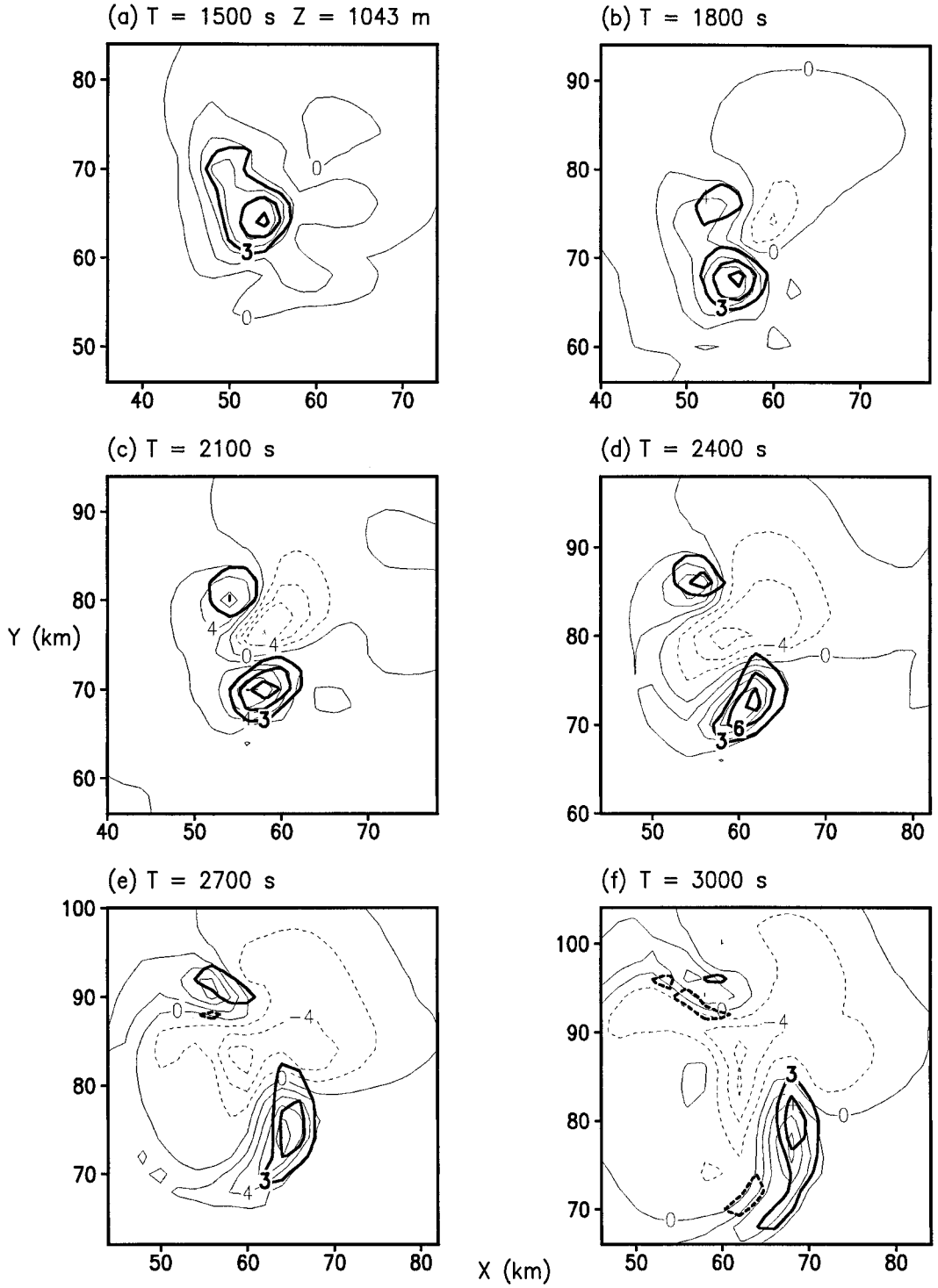

FIG. 6. Vertical motion (contoured every 2 m s^{-1}), thin contours, along with $\{-\theta_0 \partial \pi^*/\partial z + [(\theta_v - \theta_0]/\theta_0 - r_c]g\} \times 10^2$ (contoured every 3 m s^{-2}), thick contours, from (a) 1500, (b) 1800, (c) 2100, (d) 2400, (e) 2700, and (f) 3000 s at 1043 m.

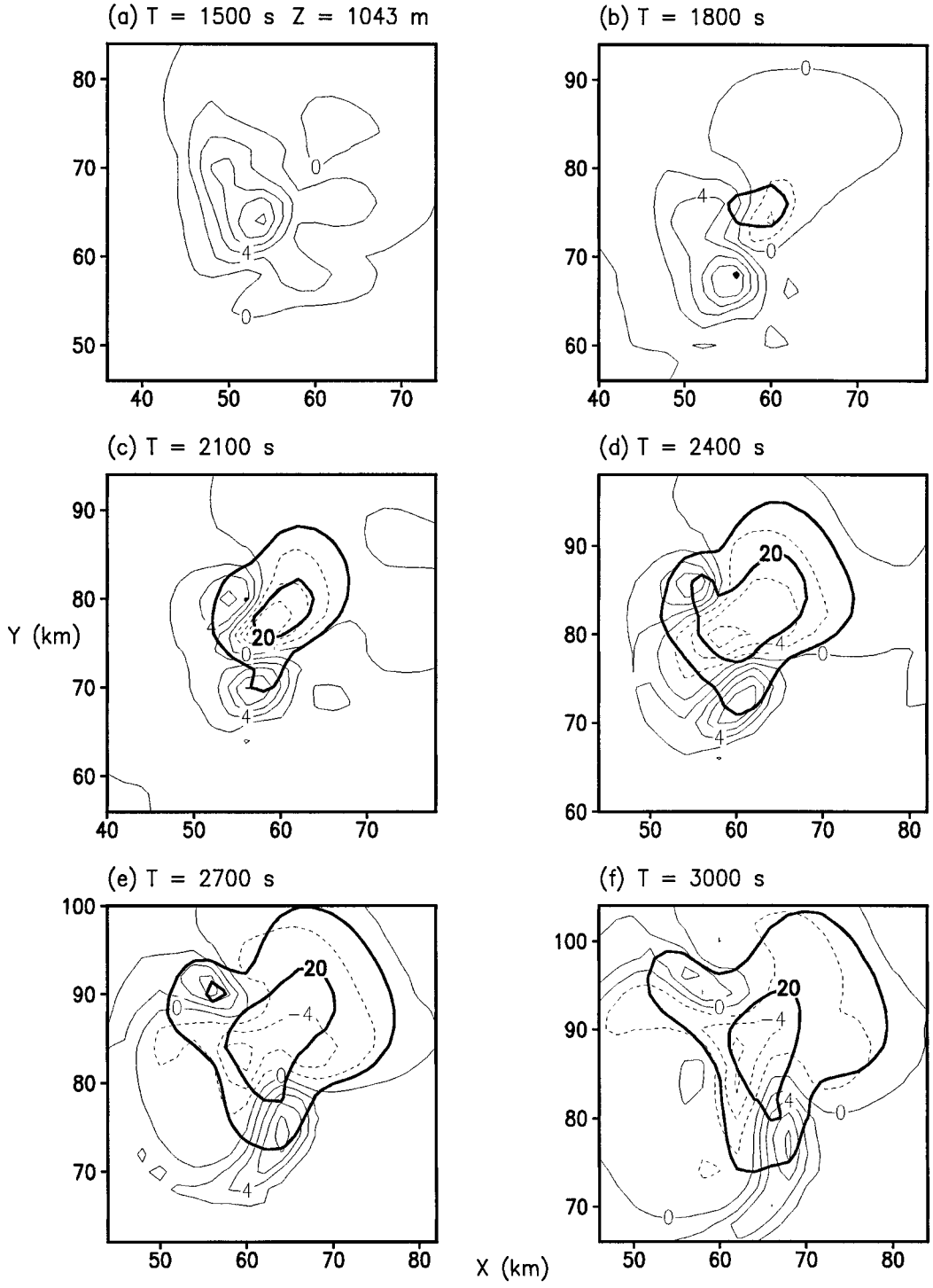

FIG. 7. Vertical motion (contoured every 2 m s^{-1}), thin contours, along with $(-\theta_0 \partial \pi^*/\partial z) \times 10^2$ (contoured every 10 m s^{-2}), thick contours, from (a) 1500, (b) 1800, (c) 2100, (d) 2400, (e) 2700, and (f) 3000 s at 1043 m.

3a–c), within the left-moving updraft, was dominated by buoyant lifting. From 2400 to 3000 s buoyant lifting decreased continuously (Figs. 5c–f). Therefore the total upward forcing during the time period between 2400 and 3000 s (Figs. 3d–f) was a result of lifting by vertical gradient in π^* (Figs. 4d–f). That is, the decay of the left-moving updraft may be a result of a decrease of upward buoyant forcing. To lend further support to this conclusion, an analysis of the updraft at lower levels was conducted.

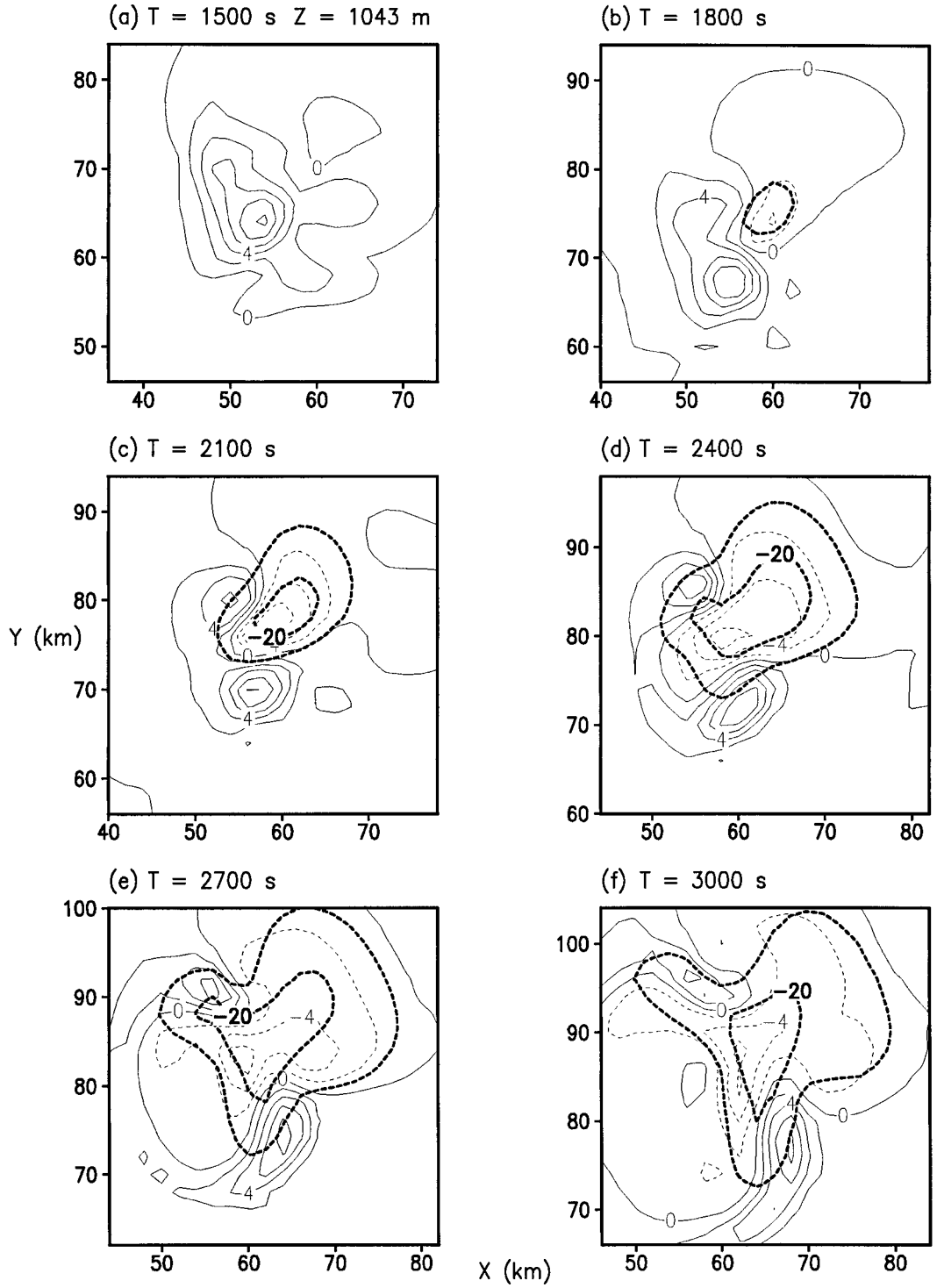

FIG. 8. Vertical motion (contoured every 2 m s^{-1}), thin contours, along with $\{[(\theta_v - \theta_0)/\theta_0 - r_c]g\} \times 10^2$ (contoured every 10 m s^{-2}), thick contours, from (a) 1500, (b) 1800, (c) 2100, (d) 2400, (e) 2700, and (f) 3000 s at 1043 m.

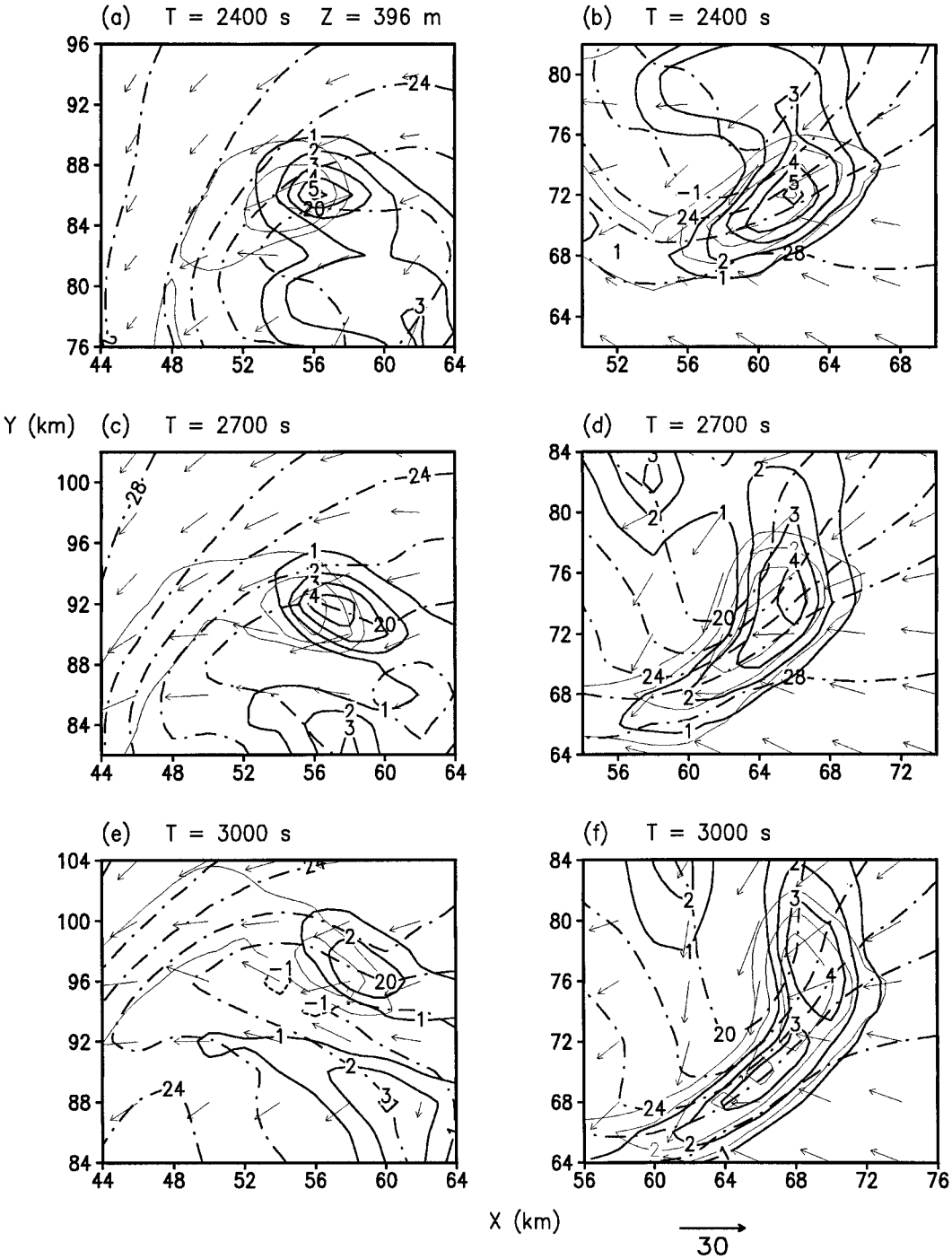

FIG. 9. Vertical motion (every 1 m s^{-1}), thin contours, along with $\{-\theta_0\partial\pi^*/\partial z + [(\theta_v - \theta_0)/\theta_0 - r_c]g\} \times 10^2$ (every 10 m s^{-2}), thick contours, and temperature (dash–dot, every 2°C), and with the left-moving storm-relative winds at (a) 2400, (c) 2700, and (e) 3000 s and the right-moving storm-relative winds at (b) 2400, (d) 2700, and (f) 3000 s at 396 m.

Near 1 km, the evolution of the total forcing (Fig. 6) was similar to that exhibited in Fig. 3. A few differences within the left-moving updraft did exist, however. During the time period between 2100 and 2400 s total upward lifting decreased near 2 km (Figs. 3c,d) while the upward forcing increased near 1 km (Figs. 6c,d). After 2400 s, the total upward forcing began to decrease (Figs. 6e,f). During the same time period, a region of downward forcing expanded over the southwest portions of the left-moving cell.

The increase in the total lifting between 2100 and 2400 s on the right side of the left mover can be ex-

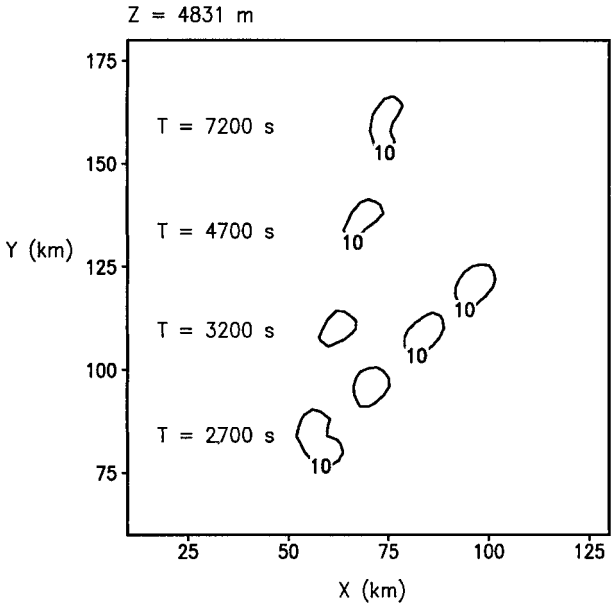

FIG. 10. Same in Fig. 2 for the no-precipitation simulation.

plained by lifting from vertical gradients in π^*. As seen in Figs. 7c and 7d, a local maximum in upward forcing developed in that region. In general, upward forcing near the updraft center of the left mover was larger than the right mover between 2400 and 2700 s (Figs. 7d,e). This result is inconsistent with linear theory, which predicts larger lifting over the right mover.

By 2100 s the region of downward buoyant forcing had expanded over the left-moving updraft (Fig. 8c). As the simulation continued, the buoyant forcing continued to decrease within the left mover. The negatively buoyant air also continued to expand northwest, faster than the low-level updraft associated with the left mover. After 2700 s (Figs. 8e,f) most of the left-moving updraft was composed of negatively buoyant air. Although buoyant forcing did decrease over portions of the right mover, the negatively buoyant air did not expand fast enough to completely overtake the right mover updraft region. This result suggests that there was, in a storm-relative frame, inflow from the undisturbed environment toward the right mover and not the left mover. A plot of the left and right mover storm-relative winds, approximately 400 m above the ground, is shown in Fig. 9 at 2400, 2700, and 3000 s. Storm motion for the left mover was approximately $U_{\rm lm} = 3.3$ m s^{-1} and $V_{\rm lm} = 18.3$ m s^{-1}. The motion of the right mover was approximately $U_{\rm rm} = 11.0$ m s^{-1} and $V_{\rm rm} = 6.6$ m s^{-1}. These values were computed during the time period from 2400 to 3000 s. This figure supports the claim that the inflow for the left-moving cell was from the forward-flanking downdraft (Figs. 9a, 9c, and 9f). This configuration was in contrast to the right mover that experienced inflow from the downdraft and the undisturbed environment (Figs. 9b, 9d, and 9f). During the time interval shown in Fig. 9, the left mover consistently existed within a colder environment compared to the right mover.

Analysis of the vertical forcing terms near and below 1 km suggest that the dissipation of the left-moving updraft was a result of the ingestion of cool air from the downdraft. Further conformation may be gained by rerunning the above simulation without the formation of a downdraft. By eliminating falling precipitation, negatively buoyant air will not be able to form through evaporative cooling. There is still the possibility that the clockwise turning of the environmental wind shear vectors below approximately 2 km may have aided in the decay of the left-moving updraft.

4. Simulated convection without precipitation

Was the initial demise of the left moving updraft at 2400 s due to the linear effect found in the study by Rotunno and Klemp (1982)? To help answer this question, a simulation was run as before except precipitation was not allowed to fall. This was accomplished by allowing water vapor to condense and form cloud water while conversions to precipitation sized particles were turned off. A time sequence of the updraft field, similar to Fig. 2, is shown in Fig. 10. This figure shows that the left-moving updraft was long lived. Therefore, the linear effects associated with the environmental shear vectors veering with height below 2 km did not cause the decay of the left mover displayed in Fig. 2.

An examination of the hodograph (Fig. 1) shows that above approximately 2 km the shear vectors turn counterclockwise with height. Linear theory predicts that clockwise-turning shear vectors with height would cause an enhancement of the right-moving updraft over the left mover. As shown in Fig. 10, however, the left mover had updraft speeds that were comparible to the right mover. Counterclockwise-turning shear vectors with height would cause an enhancement of the left mover over the right mover. Again, with no precipitation, both updrafts had similar updraft strengths throughout the simulation. As a result, one can conclude that the influence of the turning shear vectors had little influence on right- and left-moving updraft strength and longevity.

Just below 2 km the total upward lifting within the left-moving updraft increased uniformly from 1500 to 3000 (Fig. 11). The magnitude of upward forcing was similar in both updrafts. Upward forcing due to vertical gradients in π^* also increased uniformly in both the right- and left-moving updrafts (Fig. 12). There was no apparent bias toward either the right or left mover. This further supports that conclusion that the turning environmental shear vectors had little influence on either updraft. Further, near 2 km, the hodograph displayed an inflection of curvature and was somewhat linear. Linear theory does predict symmetric upward forcing as displayed in Fig. 12. Buoyant lifting was similar for both updrafts during the 1500 to 3000 s period (Fig. 13). The main difference between Figs. 13 and 5 is that the buoy-

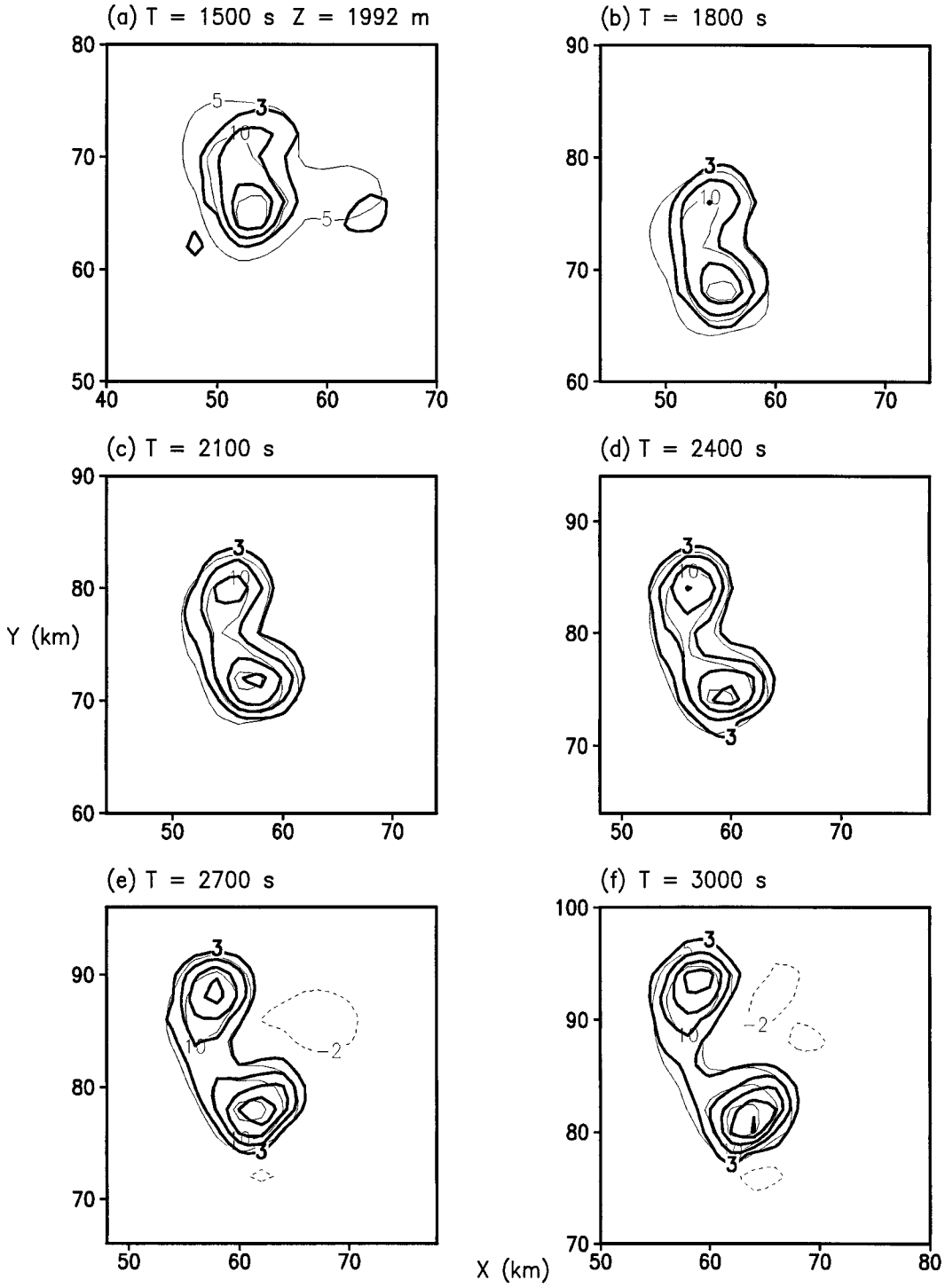

FIG. 11. Same as Fig. 3 for the no-precipitation simulation.

ant lifting did not decrease after 2400 s for the no-precipitation simulation.

Near 1 km, the total forcing did exhibit a bias toward the right-moving updraft (Fig. 14). Lifting due to vertical gradients in π^* also displayed a bias toward the right mover (Fig. 15). Larger lifting within the right mover is constent with linear theroy. The environmental shear vectors did turn clockwise with height at this level. The rightward bias, however, was not large enough to cause the dissipation of the left mover. Perhaps the depth

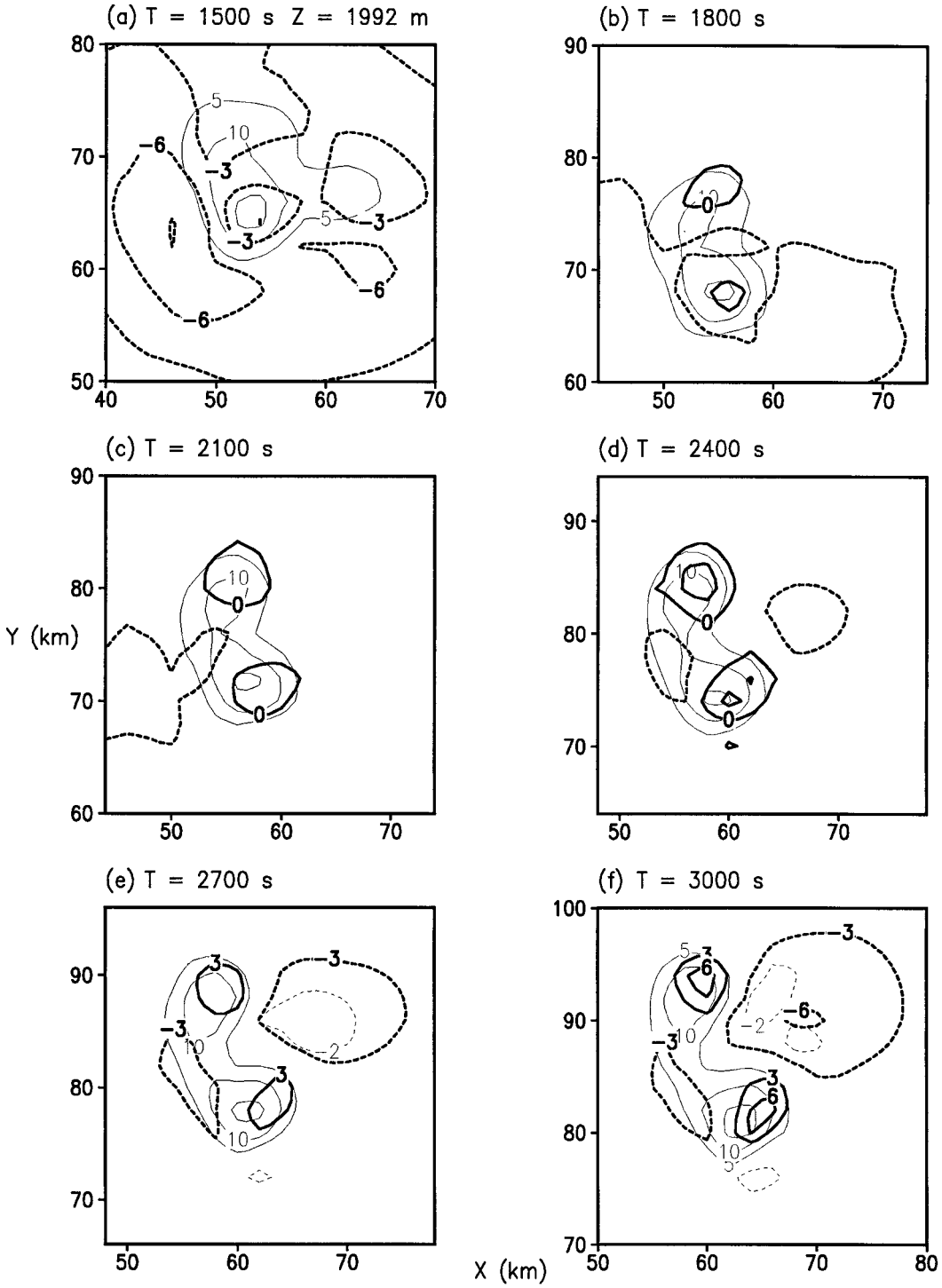

FIG. 12. Same as Fig. 4 for the no-precipitation simulation.

over which the shear vectors veered with height was too small. Values of upward buoyant forcing near 1 km was somewhat steady in both updrafts after 1800 s (Fig. 16). A comparison of this figure with Fig. 8 shows that the main difference between both simulations was a reversal of direction in which the buoyant forcing acted.

5. Discussion

Linear theory predicts the right-/left-moving updraft to dominate the left-/right-moving updraft when the shear vectors veer/back with height. The hodograph used in this study exhibited veering shear vectors below

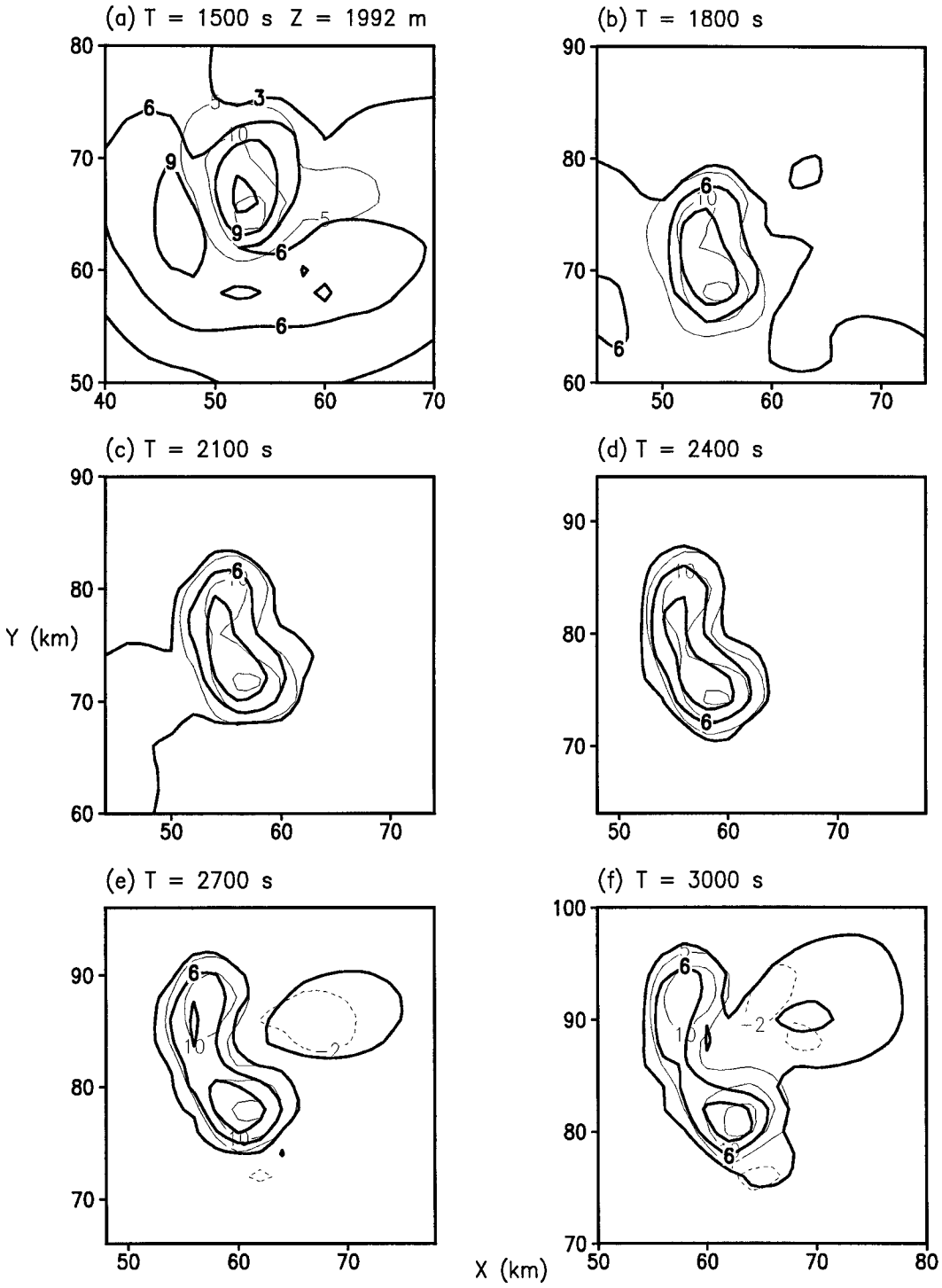

FIG. 13. Same as Fig. 5 for the no-precipitation simulation.

2 km and backing above. As a result, the development of a dominant updraft was uncertain. In the simulation with no precipitation the upward lifting by vertical gradients of π^* were somewhat similar in magnitude near 2 km (Fig. 12) for both updrafts. At lower levels a rightward bias existed (Fig. 15). Both of these results are consistent with linear theory.

However, when precipitation was allowed to fall, symmetry was not evident between both updrafts near 2 km (Fig. 4). At lower levels a rightward bias was also

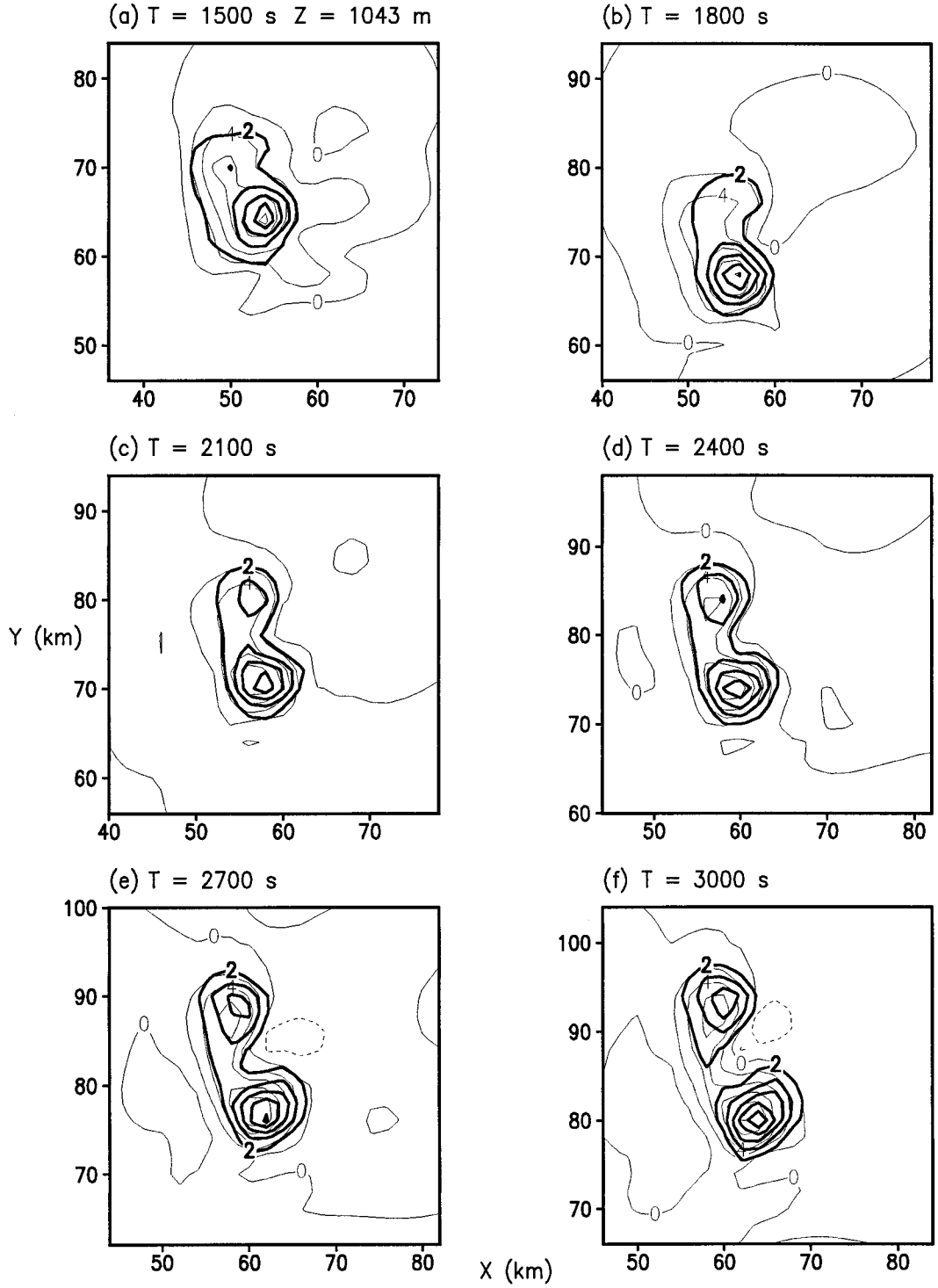

FIG. 14. Vertical motion (contoured every 2 m s^{-1}), thin contours, along with $\{-\theta_0 \partial \pi^*/\partial z + [(\theta_v - \theta_0)/\theta_0 - r_c]g\} \times 10^2$ (contoured every 2 m s^{-2}), thick contours, from (a) 1500, (b) 1800, (c) 2100, (d) 2400, (e) 2700, and (f) 3000 s at 1043 m.

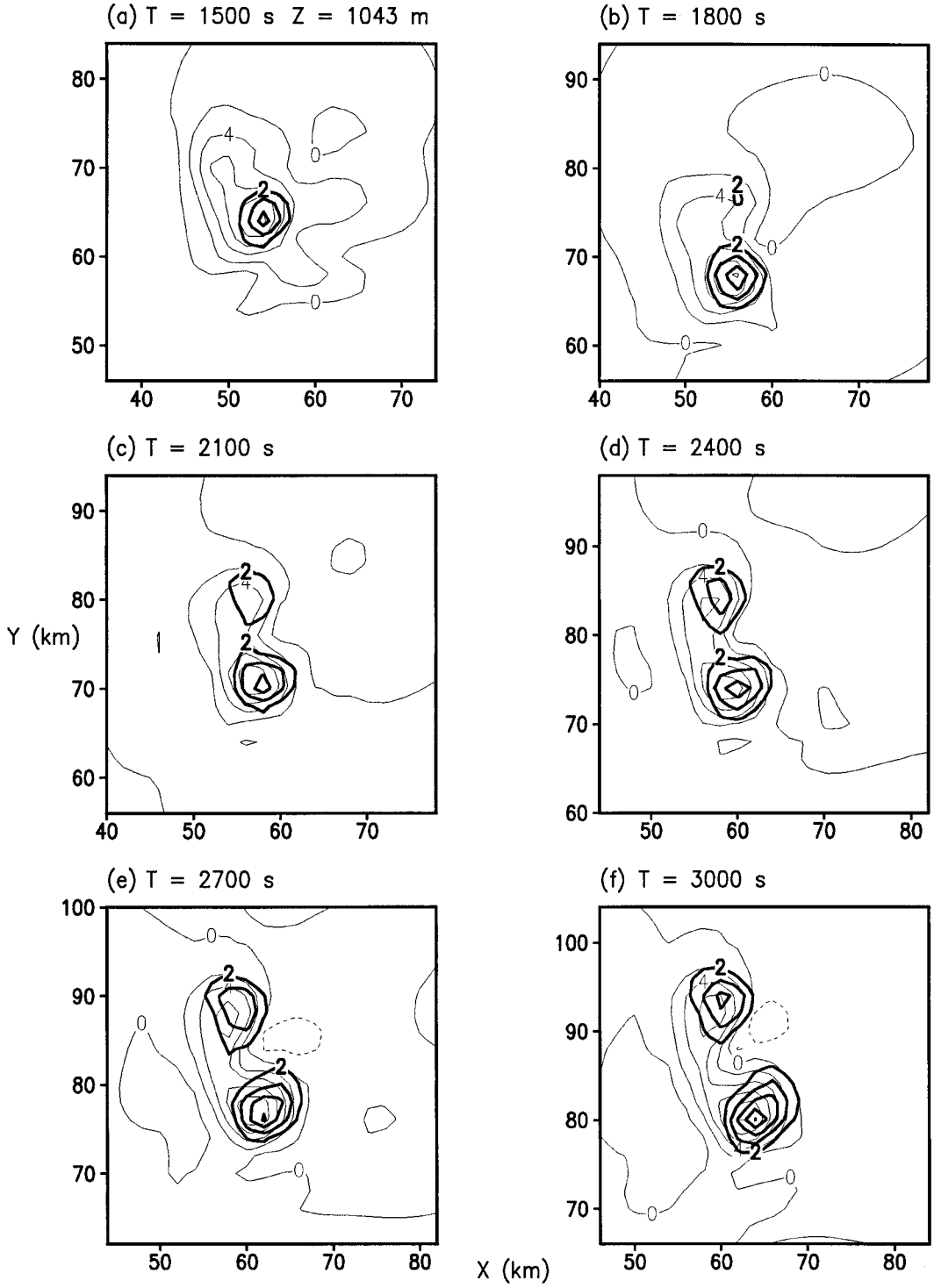

FIG. 15. Vertical motion (contoured every 2 m s^{-1}), thin contours, along with $(-\theta_0 \partial \pi^*/\partial z) \times 10^2$ (contoured every 2 m s^{-2}), thick contours, from (a) 1500, (b) 1800, (c) 2100, (d) 2400, (e) 2700, and (f) 3000 s at 1043 m.

not evident (Fig. 7). In fact, Figs. 7d and 7e suggest that the left mover displayed larger lifting than the right mover. Both of these results are not predicted by linear theory, suggesting the existence of nonlinear processes associated with the precipitating downdraft. The left-moving updraft was characterized by a continual decrease of upward buoyant forcing after 2400 s near 2 km (Fig. 5) and by negative buoyant forcing near 1 km

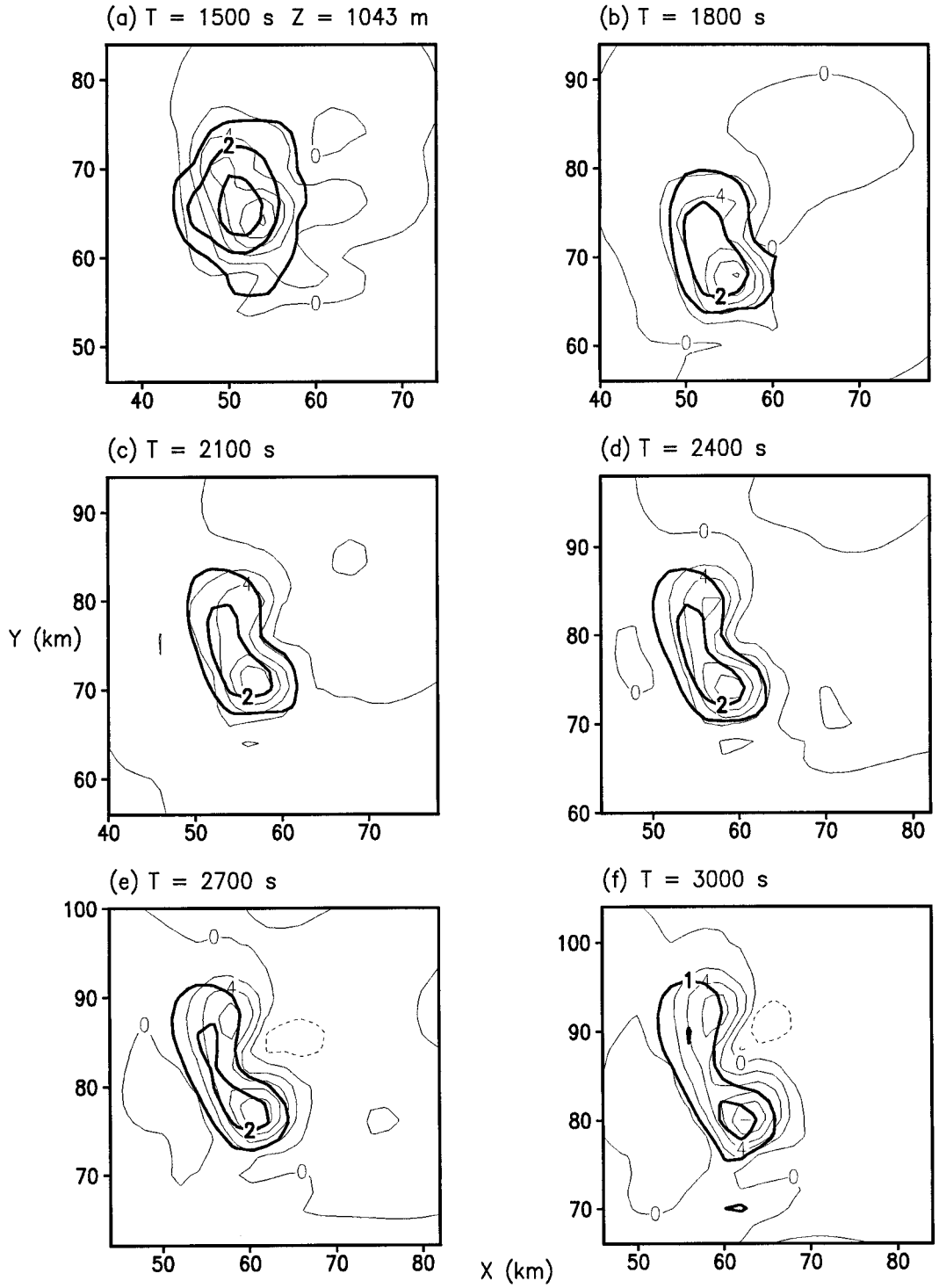

FIG. 16. Vertical motion (contoured every 2 m s^{-1}), thin contours, along with $\{[(\theta_v - \theta_0)/\theta_0 - r_c]g\} \times 10^2$ (contoured every 1 m s^{-2}), thick contours, from (a) 1500, (b) 1800, (c) 2100, (d) 2400, (e) 2700, and (f) 3000 s at 1043 m.

after 2100 s (Fig. 8). The total vertical forcing became negative over most of the left-moving updraft in the lowest few hundred meters above ground. In contrast, total vertical forcing remained positive within the right-moving updraft in the same layer. Left-moving storm-relative flow (Fig. 9) indicated that air entering the updraft originated from the downdraft. The downdraft contained colder air from evaporation of precipitation. These results suggest that the decay of the simulated left-moving updraft was due to the low-level updraft ingesting evaporatively cooled downdraft air.

As was shown in a study by Weisman and Klemp (1984), the π^* field has a contribution from the buoyancy and wind fields. That is, π^* can be written as $\pi^* = \pi^*_{\text{buo}} + \pi^*_{\text{dyn}}$, where π^*_{buo} and π^*_{dyn} are solutions of

$$\frac{\partial}{\partial x_i}\left(\rho_0\theta_0\frac{\partial \pi^*_{\text{buo}}}{\partial x_i}\right) = \frac{\partial}{\partial z}(\rho_0 B) \quad \text{and} \tag{1}$$

$$\frac{\partial}{\partial x_i}\left(\rho_0\theta_0\frac{\partial \pi^*_{\text{dyn}}}{\partial x_i}\right) = -\rho_0 d_{ij}d_{ij} + \frac{\rho_0}{2}\omega_j\omega_j + \rho_0 W^2\frac{d^2}{dz^2}(\ln\rho_0), \tag{2}$$

respectively. As a result, the two vertical forcing terms presented in this paper can be analyzed in the recasted form

$$-\theta_0\frac{\partial \pi^*_{\text{dyn}}}{\partial z} - \left[\theta_0\frac{\partial \pi^*_{\text{buo}}}{\partial z} - \left(\frac{\theta_v - \theta_0}{\theta_0} - r_c\right)g\right]. \tag{3}$$

The ability to separate the dynamic and buoyant forces acting on vertical motion represents an advantage over the method used in this paper. The analysis in this paper does, however, supply evidence that the left mover dissipated as a result of ingesting cold downdraft air as opposed to the influence of the shear vectors turning clockwise with height. As a result, the decompostion of π^* may be used in future studies.

6. Summary and conclusions

Previous idealized simulations have shown that mid-level vertical vorticity dynamically lowers the pressure on the flanks of rising updrafts in a sheared environment. The low pressure regions have been shown to enhance the lifting locally and to cause the formation of two distinct updrafts: the left and right movers. Soon after the splitting process, observations indicate that the left-moving cell generally dissipates. The predominance of right movers over left movers has been attributed to the veering of the environmental shear vectors with height. This effect is a property of the storms' environment. Linear theory predicts a high–low pressure couplet along the downshear direction in response to the updrafts interaction with the environmental shear. In that setting the pressure field is proportional to $\mathbf{S}\cdot\nabla_h w$. To better understand this process, past simulations have been conducted with and without falling precipitation to further support the claim that this linear effect does, in most cases, cause the dissipation of the left mover.

In this study a simulation was presented where the left-moving updraft did dissipate soon after the splitting process was complete. This occured in an environment in which the shear vectors veered with height below approximately 2 km. To test if the linear effect was indeed the cause of the dissipation of the left mover, the simulation was repeated, but for the case where precipitation-sized particles were not allowed to form. In that test the left mover did not dissipate soon after splitting but remained as strong as the right mover throughout the entire simulation. This result suggested that other processes caused the decay of the left-moving updraft.

An examination of the low-level buoyancy field revealed that, in a left-moving storm-relative frame, the left-moving updraft ingested cool downdraft air. This air was negatively buoyant as a result of precipitation. Over time buoyancy values decreased within the left-moving updraft near 1 km as the downdraft continued to mature. Near 2 km, the left-moving updraft contained positively buoyant air. After precipitating downdraft formed upward buoyant lifting continually decreased within the left mover. In the lowest few hundred meters the total vertical forcing became negative only within the updraft of the left-moving cell. The complete decay of the left-moving updraft soon followed. In contrast, the right-moving updraft was partially supplied with inflow from the undisturbed environment. These results were confirmed in two other simulations using smaller bubbles to trigger convection.

This study hopes to expand the work of others by introducing a process, distinct from the linear pressure effect, that may play a role in the dissipation of some left-moving updrafts. General conclusions based on this one simulation cannot be made. The purpose of this study may be viewed as an introductory one. More numerical simulations are needed to gain insight about general statements concerning the decay of observed left-moving updrafts by ingestion of cool downdraft air.

Acknowledgments. This material is based on work supported by the National Oceanic and Atmospheric Administration under Grant NA67RJ0152. The author would like to thank Dr. Mark DeMaria and Dr. Dave Nolan for their helpful comments. Thanks are also extended to Dr. Joe Klemp, who acted as a reviewer, and other anonymous reviewers.

REFERENCES

Arakawa, A., and V. Lamb, 1981: A potential enstrophy and energy conserving scheme for the shallow water equations. *Mon. Wea. Rev.,* **109,** 18–36.

Davies-Jones, R. P., 1985: Tornado dynamics. *Thunderstorm Morphology and Dynamics,* 2d ed., E. Kessler, Ed., University of Oklahoma Press, 197–236.

Grasso, L. D., and W. R. Cotton, 1995: Numerical simulation of a tornado vortex. *J. Atmos. Sci.,* **52,** 1192–1203.

Klemp, J. B., and R. B. Wilhelmson, 1978: The simulation of three-dimensional convective storm dynamics. *J. Atmos. Sci.,* **35,** 1070–1096.

Lilly, D. K., 1962: On the numerical simulation of buoyant convection. *Tellus,* **14,** 148–172.

Pielke, R. A., and Coauthors, 1992: A comprehensive meteorological modeling system-RAMS. *Meteor. Atmos. Phys.,* **49,** 69–91.

Rotunno, R., and J. B. Klemp, 1982: The influence of the shear-induced pressure gradient on thunderstorm motion. *Mon. Wea. Rev.,* **110,** 136–151.

——, and ——, 1985: On the rotation and propagation of simulated supercell thunderstorms. *J. Atmos. Sci.,* **42,** 271–292.

Schlesinger, R. E., 1980: A three-dimensional numerical model of an isolated thunderstorm. Part II: Dynamics of updraft splitting and mesovortex couplet evolution. *J. Atmos. Sci.,* **37,** 395–420.

Smagorinsky, J., 1963: General circulation experiments with the primitive equations. Part 1: The basic experiment. *Mon. Wea. Rev.,* **91,** 99–164.

Tripoli, G. J., and W. R. Cotton, 1981: The use of ice-liquid water potential temperature as a thermodynamic variable in deep atmospheric models. *Mon. Wea. Rev.,* **109,** 1094–1102.

——, and ——, 1982: The Colorado State University three-dimensional cloud mesoscale model, 1982. Part I: General theoretical framework and sensitivity experiments. *J. Rech. Atmos.,* **16,** 185–220.

Walko, R. L., W. R. Cotton, M. P. Meyers, and J. Y. Harrington, 1995: New RAMS cloud microphysics parameterization. Part I: The single moment scheme. *Atmos. Res.,* **38,** 29–62.

Weisman, M. L., and J. B. Klemp, 1984: The structure and classification of numerically simulated convective storms in directionally varying wind shear. *Mon. Wea. Rev.,* **112,** 2479–2498.

Wilhelmson, R. B., and J. B. Klemp, 1981: A three-dimensional numerical simulation of splitting severe storms on 3 April 1964. *J. Atmos. Sci.,* **38,** 1581–1600.